GEOPHYSICS, VOL. 62, NO. 4 (JULY-AUGUST 1997); P. 1163–1176, 14 FIGS., 3 TABLES.

Effects of pore and differential pressure on compressional wave velocity and quality factor in Berea and Michigan sandstones

Manika Prasad* and Murli H. Manghnani‡

ABSTRACT

Compressional-wave velocity (V_P) and quality factor (Q_P) have been measured in Berea and Michigan sandstones as a function of confining pressure (P_c) to 55 MPa and pore pressure (P_p) to 35 MPa. V_P values are lower in the poorly cemented, finer grained, and microcracked Berea sandstone. Q_P values are affected to a lesser extent by the microstructural differences. A directional dependence of Q_P is observed in both sandstones and can be related to pore alignment with pressure. V_P anisotropy is observed only in Berea sandstone. V_P and Q_P increase with both increasing differential pressure ($P_d = P_c - P_p$) and increasing P_p. The effect of P_p on Q_P is greater at higher P_d. The results suggest that the effective stress coefficient, a measure of pore space deformation, for both V_P and Q_P is less than 1 and decreases with increasing P_d.

INTRODUCTION

Knowledge about the pore and confining pressure dependences of the compressional-wave velocity (V_P) and attenuation (Q_P^{-1}) in reservoir rocks is an important prerequisite for relating laboratory measurements to in-situ rock properties, and for interpreting seismic measurements in terms of subsurface petrophysical parameters. The effect of pore pressure (P_p) on velocity and attenuation is of special interest, since high pore pressures that are nearly equal to lithostatic pressures can be encountered in beds that are bound by impermeable rocks (Green and Wang, 1986). The importance of pore and confining pressures on compressional-(V_P) and shear-wave (V_S) velocities in various types of sedimentary rocks (e.g., sandstones, chalk) has been reported (Brandt, 1955; Christensen and Wang, 1985; Coyner and Cheng, 1985; Gangi, 1991) where velocities were found to be dependent upon effective pressure $P_e = P_c - nP_p$, n being the effective stress coefficient. Some studies have also related effective stress to fluid permeability k (Zoback and Byerlee, 1975; Bernabé, 1987; Berryman, 1992). Since permeability can be a dominant factor in controlling loss mechanisms in porous media (Biot, 1956a and b; Stoll, 1989; Akbar et al., 1993), a study of the quality factor Q (or attenuation, Q^{-1}) as a function of both confining and pore pressures is of special interest in seismic exploration for oil. It has been speculated that high pore pressure would lead to low velocity and Q values caused by decreased effective pressures (Green and Wang, 1986). On the basis of velocity dispersion results, Winkler (1985; 1986) has predicted that saturated samples are more likely to resemble an undrained condition at higher (ultrasonic) frequencies. Since the pore fluid pressure generated during the short duration of an acoustic pulse does not have enough time to equilibrate, the rock will be in an unrelaxed state. In this state, the higher stiffness will contribute to higher velocities. Although the effect of pore pressure on velocity has been studied in various rock types (e.g., Jones and Nur, 1983; Gangi, 1991), its effect on attenuation is mostly unknown. Investigation of the effect of pore fluid pressure on attenuation properties of candidate reservoir rocks is particularly important for evaluating the reservoir properties. For example, the seismic inference of pore pressure buildups could provide useful information about the fluid content and pore geometry of a reservoir (Green and Wang, 1986). The purposes of this study are (1) to present compressional wave velocity (V_P) and quality factor (Q_P) for two specimens of Berea and Michigan sandstones, measured as a function of confining (P_c) and pore pressures (P_p), and (2) to discuss the implications of an effective pressure law for lithological interpretations of seismic data.

Published on "Geophysics Online" May 6, 1997. Manuscript received by the Editor March 24, 1994; revised manuscript received July 30, 1996.
*Formerly Mineral Physics Group, Hawaii Institute of Geophysics and Planetology, School of Earth and Ocean Science and Technology, University of Hawaii, HI 96822; presently SRB Project, Department of Geophysics, Stanford University, Stanford, California 94305-2215. E-mail: manika@pangea.stanford.edu.
‡Mineral Physics Group, Hawaii Institute of Geophysics and Planetology, School of Earth and Ocean Science and Technology, University of Hawaii, HI 96822.

EXPERIMENTAL PROCEDURE

Samples

Cube specimens of 18 mm length on each side were prepared from Berea and Michigan sandstones. The faces were ground on a glass plate and cleaned with a water jet and in an ultrasonic bath to remove rock flour. The faces are parallel to within 20 μm. Bulk and grain densities and porosity were determined by the Archimedes method. The microstructure of the samples was examined under optical microscope and scanning acoustic microscope (Briggs, 1985, 1992; Rodriguez-Rey et al., 1990; Prasad et al., 1995).

Microstructure

Scanning acoustic microscopy micrographs of the Michigan and Berea sandstone specimens are shown in Figure 1. These results have been discussed in detail elsewhere (Prasad and Manghnani, 1996; Prasad et al., manuscript in review), and the main features are given here. The Michigan sandstone is composed of rounded grains with a grain size of about 300–400 μm, and is well cemented. The low impedance contrast between grains and cement suggests a similar (siliceous) composition of grains and cement. The grains do not show any microcracking. In contrast, Berea sandstone is composed of angular grains (150–200 μm) which show microcracks. The grain contacts are somewhat jagged and are weakly cemented. The major difference between the sandstones is seen in their contact areas between grains. In Berea sandstone, this area resembles a microcrack or an elongated pore with large aspect ratio. The contact areas in Michigan sandstone resemblence have a greater to a group of more or less equant pores. These differences in microstructure will be considered further when comparing the variations in observed velocity and attenuation values.

Other measured physical properties of the samples are given in Table 1. The Michigan sandstone has a lower porosity, larger grain size, and well cemented grains.

Ultrasonic experimental setup

The pulse transmission technique (Birch, 1960) was used for compressional-wave velocity (V_P) measurements. The quality factor (Q_P) was calculated using the spectrum division method (Toksöz et al., 1979; Johnston and Toksöz, 1980; Sears and Bonner, 1981). Measurements were made in two perpendicular directions. In Berea sandstone, the measured directions were parallel (V_{P_h}, Q_{P_h}) and perpendicular (V_{P_v}, Q_{P_v}) to the visible bedding plane. In Michigan sandstone, where no bedding was

Table 1. Physical properties of the samples.

	Berea sandstone	Michigan sandstone
Bulk density (g/cm^3)	2.282	2.362
Porosity (%)	21.18	16.94
Grain size (μm)	150–250	300–400
Permeability (md)	100	——

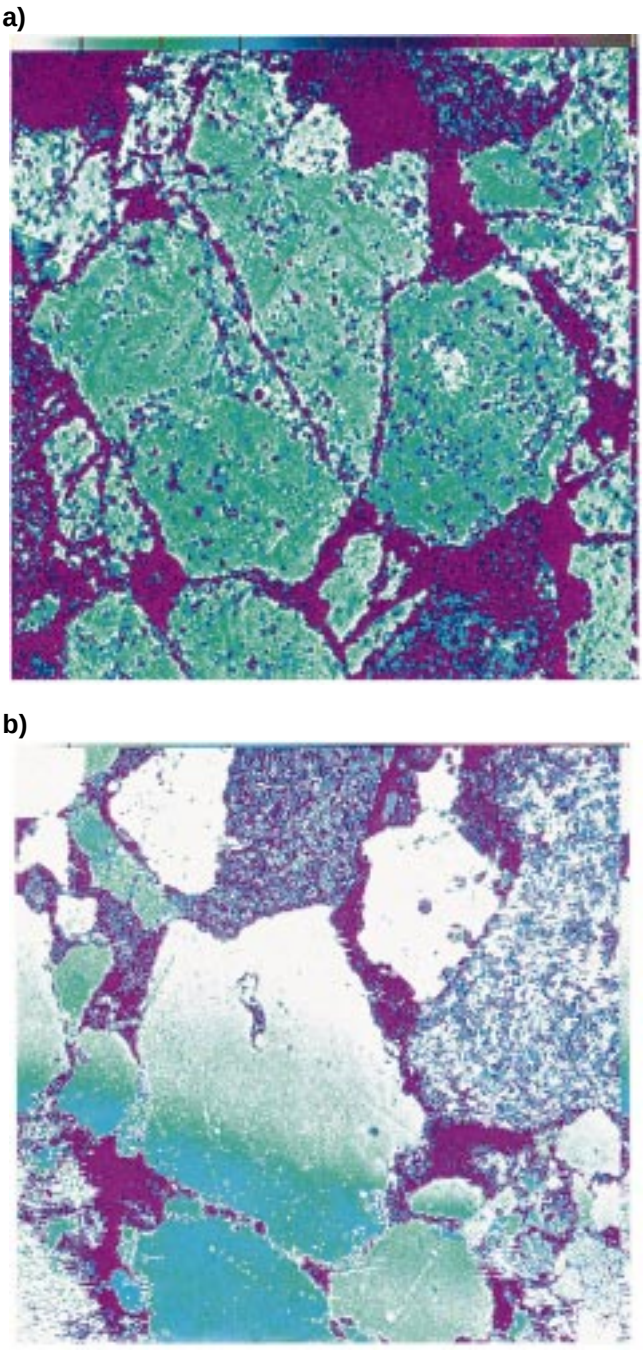

FIG. 1. Acoustic microscopy micrograph of Michigan and Berea sandstones at 1 GHz showing quartz grains, cementation, and pore structure. The scanned image of Berea sandstone (a) is 312 μm $\times$ 312 μm, that of Michigan sandstone (b) is 1000 μm $\times$ 1000 μm. Impedance contrasts in the micrograph are color coded: cyan through blue to white denote progressively higher impedance. Pore spaces and interfaces appear as cyan and blue areas. Grains are green to white colored. Michigan sandstone (b) has well cemented, rounded grains with few visible microcracks. Impedance (brightness) contrast within the grains is low. The grains in Berea sandstone (a) are angular (150–200 μm) and show microcracks. The grain contacts are somewhat jagged and are weakly cemented. The grain contacts are wider than in Michigan sandstone.

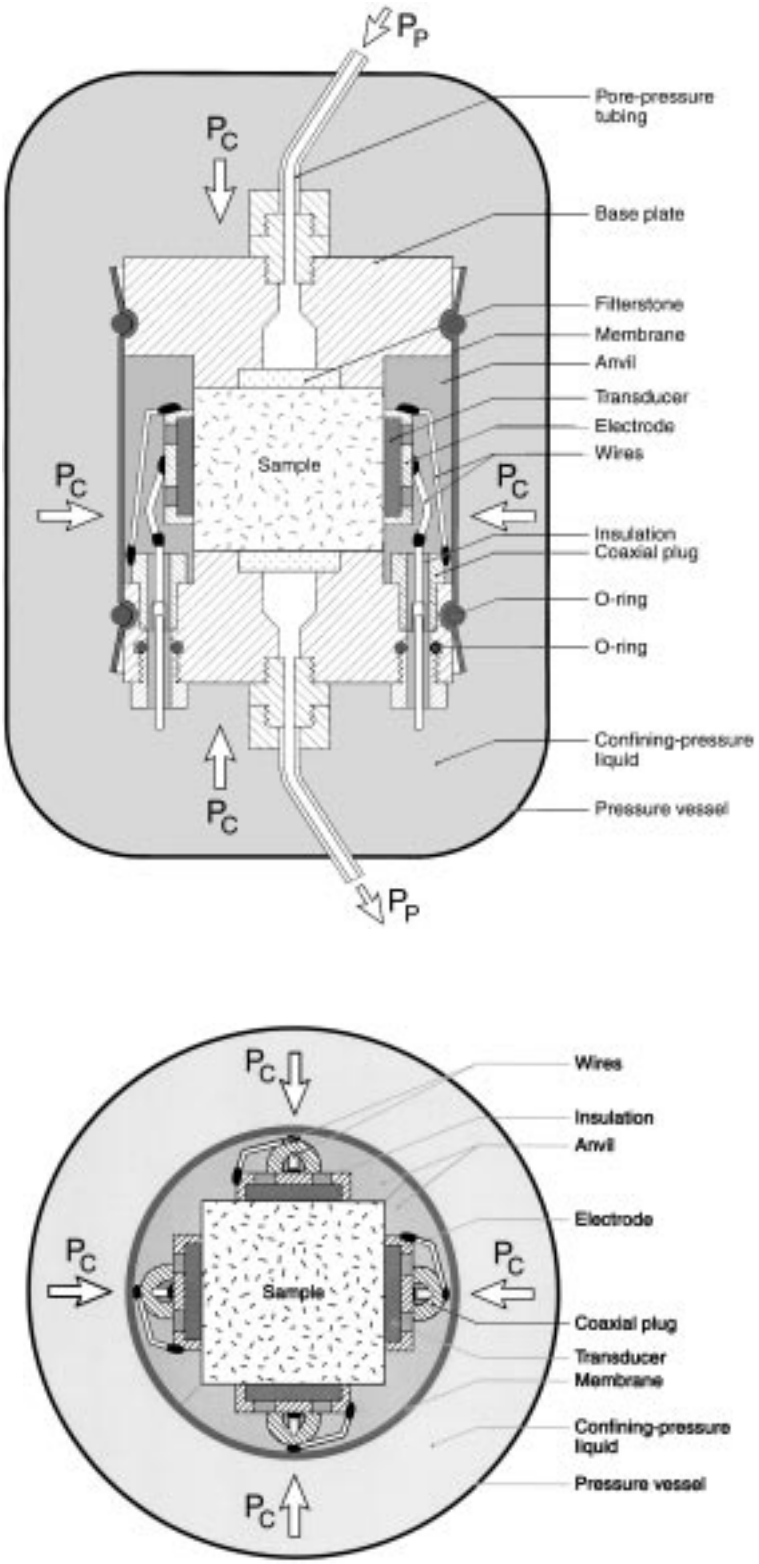

FIG. 2. Schematic diagram of the ultrasonic pulse transmission experimental setup showing details of the epoxy anvils and transducer holders.

visible, the measured directions were arbitrarily chosen as parallel (V_{P_v}, Q_{P_v}) and perpendicular (V_{P_h}, Q_{P_h}) to borehole axis.

The experimental setup consists of a digital Tektronix 7854 oscilloscope, an HP 214B pulse generator, and a preamplifier. A new sample-transducer assembly allows us to conduct the measurements in two directions in a sample under controlled pore and confining pressures. The cube sample, with 1 MHz PZT-transducers attached to the faces, is enclosed in epoxy anvils, which prevents the mixing of confining and pore fluids. The cylindrical shape formed by the anvils was covered by a latex rubber membrane and sealed with O-rings to prevent the confining pressure medium from entering the pore fluid path. A high viscosity bonding medium (Dow Corning V9) was used to bond the transducers to the sample. The transducers are placed in brass holders which, together with the epoxy, provide a backing for the transducers. The electrical leads run through conduits in the anvils. When the anvils are assembled, all four transducers are positioned on the sample faces at the same height. Filter-stones placed on the remaining two faces of the cube facilitate passage of pore fluid through the sample. Figure 2 shows details of the epoxy anvils, transducer holders, electrical and pore fluid circuits.

This configuration allowed measurements at various confining and pore pressures up to 55 and 35 MPa, respectively. The pressure limits were defined by the aluminum sample holder, electrical contacts, and the epoxy used in the anvils. The samples were saturated under a vacuum with 60 ppm brine prior to loading into the assembly.

Traveltimes were measured on the oscilloscope by digitizing a trace with 1024 points at a time sweep of 5 μs, thus allowing a time resolution of about 5 ns or about 0.2% error in velocity. Actual error in velocity measurement is estimated to be around 1% because of operator error in picking first arrival. Traveltime calibration was accomplished by using aluminum rods of different lengths. Q_P was measured by the spectral ratio technique (Toksöz et al., 1979; Johnston and Toksöz, 1980; Sears and Bonner, 1981) with the assumption of a constant Q over the bandwidth used (0.8–1.3 MHz). The signal from an aluminum cube of the same size was recorded at various pressure steps and used as a reference signal at that pressure. In this way, similar coupling and pressure conditions were maintained for the reference and sample. Figure 3 shows typical signals for aluminum, Lucite, and Berea sandstone samples along with their spectra. The signals are damped and no ringing is seen. The Q_P value for Lucite obtained from this signal was found to be 54, which is in agreement with reported values of 50 (Toksöz et al., 1979). Because of the short sample lengths, diffraction corrections were necessary (Sears and Bonner, 1981; Winkler and Plona, 1982; Wepfer and Christensen, 1990). The tables of Benson and Kiyohara (1974) and Khimunin (1972) were used for amplitude and phase corrections.

RESULTS

Differential pressure experiments

Figure 4 presents the increase in V_P with increasing differential pressure ($P_d = P_c - P_p$). A constant low pore pressure of 0.1–0.2 MPa was maintained to ensure full saturation during the experiment. Michigan sandstone, with larger grain size and lower porosity, has higher V_P values than Berea sandstone. At low P_c, up to 15 MPa, the rate of increase in V_P is higher in Berea sandstone; at higher P_c, V_P changes only slightly with P_c. In Michigan sandstone, V_P increases monotonically with increasing P_c to 40 MPa. The different behavior of V_P gives an indication of the type of pores in the samples. A steep increase in V_P at low pressures is indicative of the closure of microcracks or pores with large aspect ratios (Lo et al., 1986; Wepfer and Christensen, 1990; Prasad et al., 1994).

The V_P anisotropy is defined as

$$A_{V_P} = 200 \cdot \frac{(V_{P_h} - V_{P_v})}{(V_{P_h} + V_{P_v})} \tag{1}$$

As seen in Figure 5, the average velocity anisotropy in Michigan sandstone is low (about 1–2%) but slightly above the experimental error, and it does not vary as a function of P_d. Such a low velocity anisotropy is attributed to a lack of preferred grain orientation in its microstructure. On the other hand, Berea sandstone with visible bedding has higher velocity anisotropy (8%) and it decreases with increasing P_d and attains a value of about 4% at $P_d = 45$ MPa. Q_P increases with increasing P_d in both sandstones (Figure 6); however, the increase is somewhat higher in Michigan sandstone.

The differences in V_P and Q_P values are related to the microstructural differences (see Figure 1). The higher V_P and Q_P values measured for the Michigan sandstone can be attributed to better cementation and intact grains. The better cementation can be evaluated as higher initial contact radius which causes a higher V_P (Winkler, 1983; Prasad and Meissner, 1992). A steep gradient of V_P increase at low P_c and decrease of V_P anisotropy with P_c can be explained by deformation of elongated weak contact areas and closing of microcracks between grains in Berea sandstone (Lo et al., 1986). Michigan sandstone has stiffer contact areas that are more resistant to deformation at lower pressures.

Analogous to V_P anisotropy, Q_P anisotropy, defined as

$$A_{Q_P} = 200 \cdot \frac{(Q_{P_h} - Q_{P_v})}{(Q_{P_h} + Q_{P_v})} \tag{2}$$

shows negative values with increasing pressure ($Q_{P_v} > Q_{P_h}$, Figure 7). In Berea sandstone, Q_P anisotropy decreases to negative values as differential pressure increases above 30 MPa. A similar decrease in Q_P anisotropy with increasing confining pressure in deep sea drilling program (DSDP) sediments has been attributed to horizontally aligned water-filled elliptical pores (O'Brien et al., 1989).

Akbar et al. (1993) have shown that attenuation depends strongly on the pore orientation. Q_P is lower for wave propagation perpendicular to the long axes of elliptical pores than it is for waves traveling parallel to this direction. Using this analogy, the Q_P anisotropy observed in our experiments could be explained by the pore orientation rather than the preferred orientation of grains or bedding planes. This would also explain the low anisotropy in V_P, which is not significantly affected by pore space (O'Brien et al., 1989). Figure 8 shows acoustic microscopy micrographs of the pore space distribution in Berea sandstone. Images of two faces are shown: (a) cut perpendicular (h-direction of wave propagation) and (b) cut parallel (v-direction of wave propagation) to the visible bedding plane. The arrows in Figure 8a mark alignment of pore spaces (black colored). The image of the face cut parallel to bedding (Figure 8b) does not show any alignment of pore spaces.

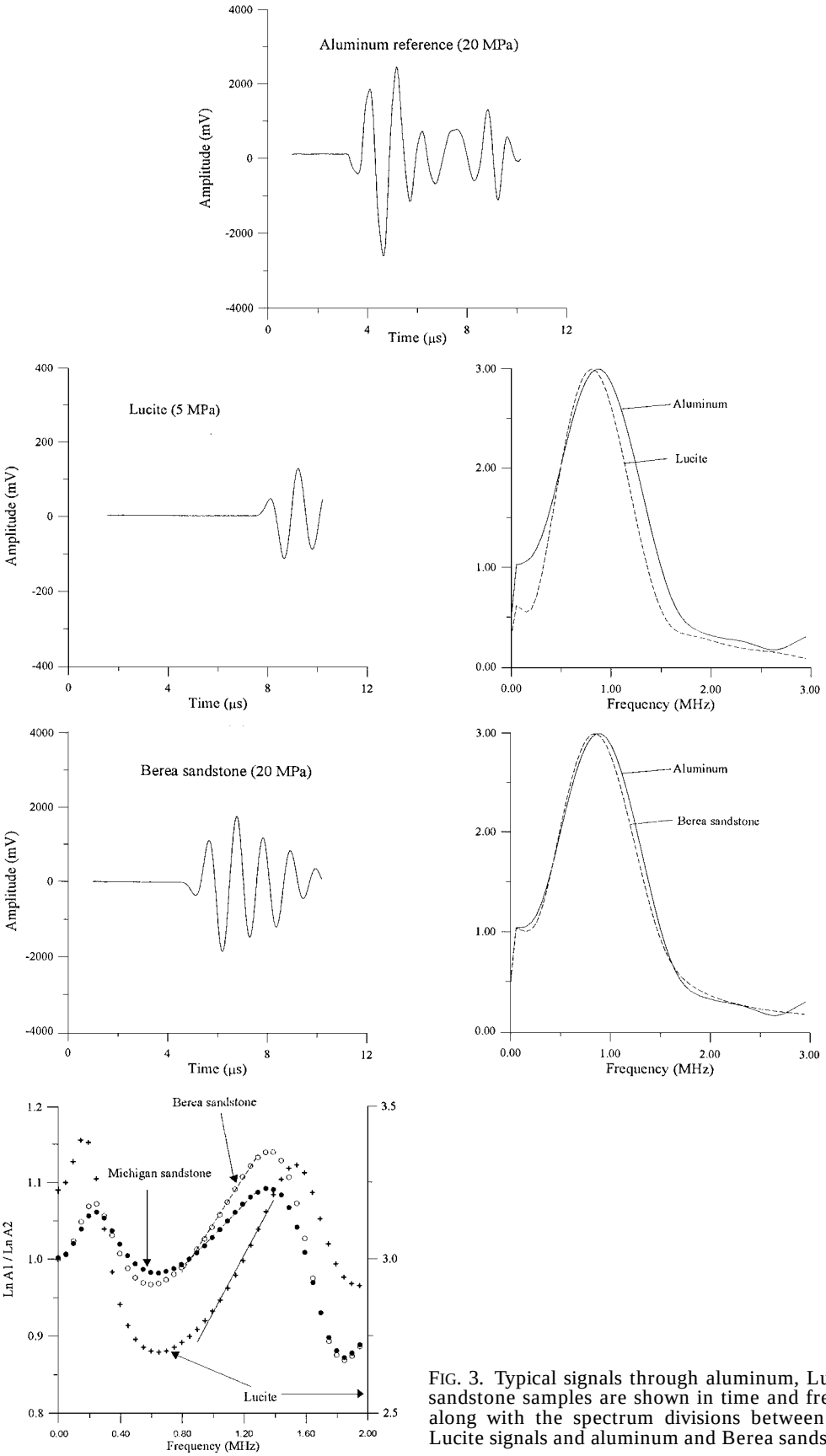

FIG. 3. Typical signals through aluminum, Lucite, and Berea sandstone samples are shown in time and frequency domain along with the spectrum divisions between aluminum and Lucite signals and aluminum and Berea sandstone signals.

This alignment of low impedance structures (pores) could be accentuated with increasing pressure and would lead to higher Q_{P_v}-values.

Effect of pore pressure

The 3-D surfaces showing the variations in V_{P_h} and Q_{P_h}, as affected by P_p and P_d for both sandstones, are presented in Figures 9 and 10. The plots are made by Matlab routines of gridding and 3-D plotting, which use a 2-D interpolation between data points to construct the grids. The velocity plots for Berea and Michigan sandstones (Figure 9) show a strong dependence of V_P on P_d in contrast to a weak dependence on P_p. The quality factor plots for both sandstones (Figure 10) show that Q_P changes not only with P_d but also with P_p. This dependence of Q_P on P_p is greater at higher P_d and is more

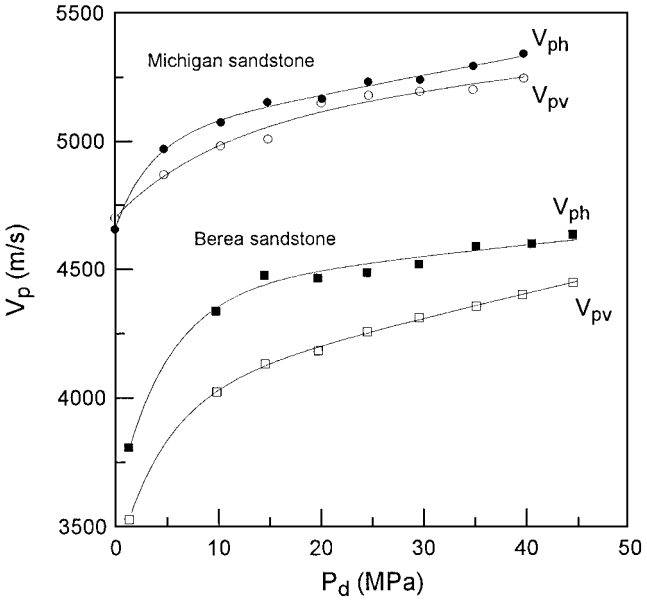

FIG. 4. V_P versus differential pressure for Berea and Michigan sandstones measured in two directions denoted by the subscripts *ph* and *pv*. Measurements were made at $P_p = 0.1$. Solid lines represent best fits obtained with the equation $V_P^2 = A + B \cdot P_d + C \cdot e^{-P_d/D}$.

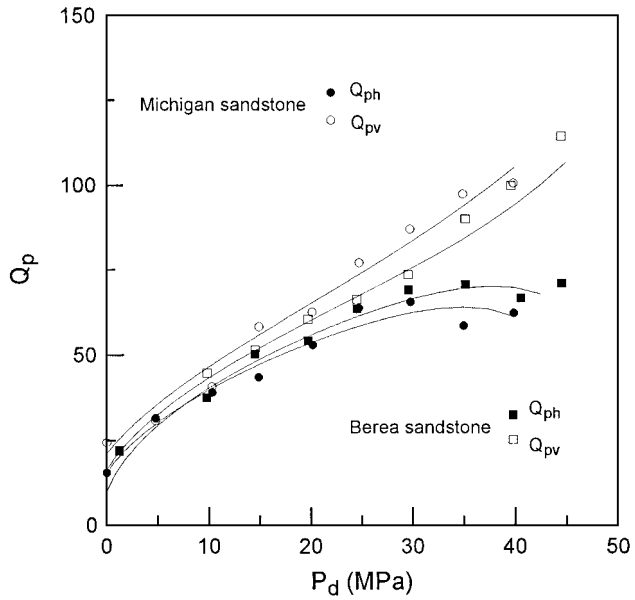

FIG. 6. Q_P versus P_d in both sandstones measured in two directions denoted by the subscripts *ph* and *pv*. Measurements were made at $P_p = 0.1$ MPa. Solid lines represent best fits obtained with the equation $Q_P^2 = A + B \cdot P_d + C \cdot e^{-P_d/D}$.

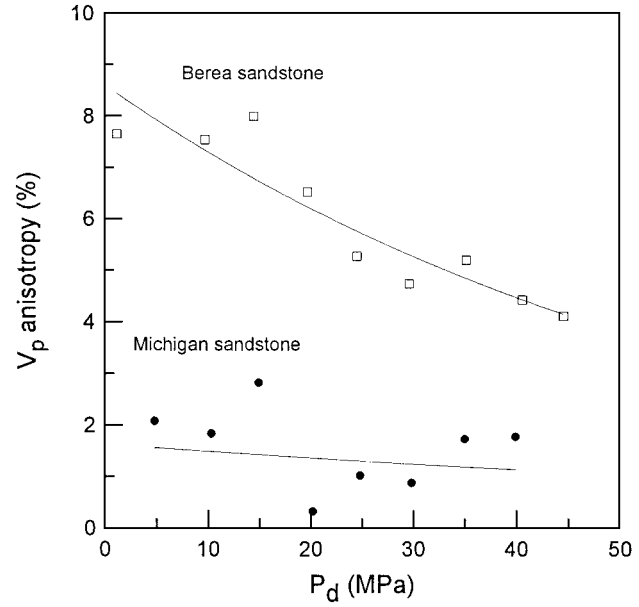

FIG. 5. V_P anisotropy versus P_d. Positive anisotropy implies that V_{P_h} is greater than V_{P_v}. Measurements were made at $P_p = 0.1$ MPa. Solid lines represent exponential fits through the data points.

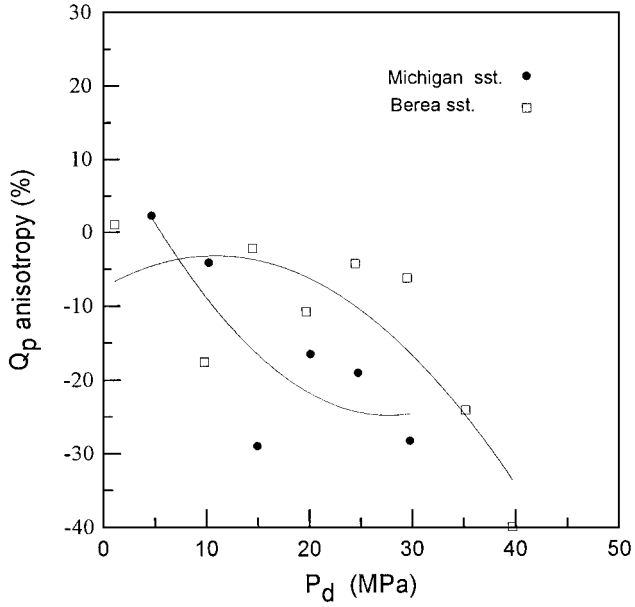

FIG. 7. Q_P anisotropy versus P_d. Positive anisotropy implies that Q_{P_h} is greater than Q_{P_v}. Measurements were made at $P_p = 0.1$ MPa. Solid lines represent second degree polynomial fits through the data points.

pronounced in the case of Michigan sandstone. The increase in V_P with increasing P_p is between 1–2% (above experimental error) and the increase in Q_P is between 15–20%.

DISCUSSION

The dependences of V_P and Q_P on both P_d and P_p suggest that the effects of P_c and P_p are not equal and opposite. Effective pressure (P_e) is used to define conditions when P_p does not exactly cancel P_c:

$$P_e = P_c - nP_p, \tag{3}$$

where n is the effective stress coefficient (Todd and Simmons, 1972; Christensen and Wang, 1985; Gangi, 1991). Differential pressure (P_d) is a special case when $n = 1$, and

$$P_d = P_e = P_c - P_p. \tag{4}$$

The observation that V_P and Q_P depend on both P_d and P_p, implies that $n \neq 1$. To test this observation, the data plotted in Figures 9 and 10 are replotted with P_p = constant, as shown for V_{P_h} in Figure 11 and for Q_{P_h} in Figure 12. Also shown are best-fit plots of the form

$$V_P^2 = A + B \cdot P_c + C \cdot e^{-P_c/D} \tag{5}$$

(Greenfield and Graham, 1994), where A, B, C, and D are constants. The velocity plots in Figure 11 show some change with increasing pore pressure. At low pore pressures, the V_P-curves are similar to the one at $P_p = 0$. At higher P_p, the change in slope at the elbow region of the V_P-curves shifts toward higher P_c-values. Furthermore, the change in slope is more gradual at higher P_p.

During the V_P and Q_P measurements at varying P_p, there was some scatter in monitored P_d values. Hence, equation (5) was used at each P_p step to interpolate V_P and Q_P values for P_d = constant. These interpolated V_P and Q_P values are plotted in Figures 13 and 14, respectively. One consequence of V_P- and Q_P-dependence on P_d and P_p is that the slope of a straight line fitted to V_P and Q_P versus P_c values at P_d = constant is not equal to 0. For V_P, the variation is in the order of 1–2%, which is slightly higher than experimental error. For Q_P, the change with P_p is much higher, between 15–20%. Furthermore, the increase in the slope of these linear fits with increasing pressure implies that this dependence on P_d and P_p is greater at higher P_d, and n changes with pressure. The factor n in the effective pressure equation (3) has been described as the effective stress coefficient or the coefficient of internal (pore space) deformation. The equation for n,

$$n = 1 - \frac{\left[\dfrac{\partial V_P}{\partial P_p}\right]_{P_d}}{\left[\dfrac{\partial V_P}{\partial P_d}\right]_{P_p}}, \tag{6}$$

(Todd and Simmons, 1972; Christensen and Wang, 1985) was then solved for V_P and Q_P in both samples. $[\partial V_P/\partial P_d]_{P_p}$ values were evaluated from the slopes for the P_p = constant curves shown in Figures 11 and 12 (see Table 2). For $[\partial V_P/\partial P_p]_{P_d}$ values, the slopes of the P_d = constant straight line fits shown in Figures 13 and 14 were evaluated. An approximation of $[\partial V_P/\partial P_d]_{P_p}$ from the V_P at $P_p = 0$ curve involves an assumption that this curve is duplicated at higher pore pressures. At higher pressure, this assumption would lead to a lower estimate of n. Table 2 shows a comparison of slopes and n values for V_P at various pressures. Two different sets are calculated from (1) V_P at $P_p = 0$ and (2) V_P at $P_p \neq 0$ curves. Referring to Figures 11 and 12 and Table 2, the slopes for $P_p = 0$ are lower than those for $P_p \neq 0$ for both sandstones. Table 3 gives the values of n calculated for V and Q at different pressures. These calculated

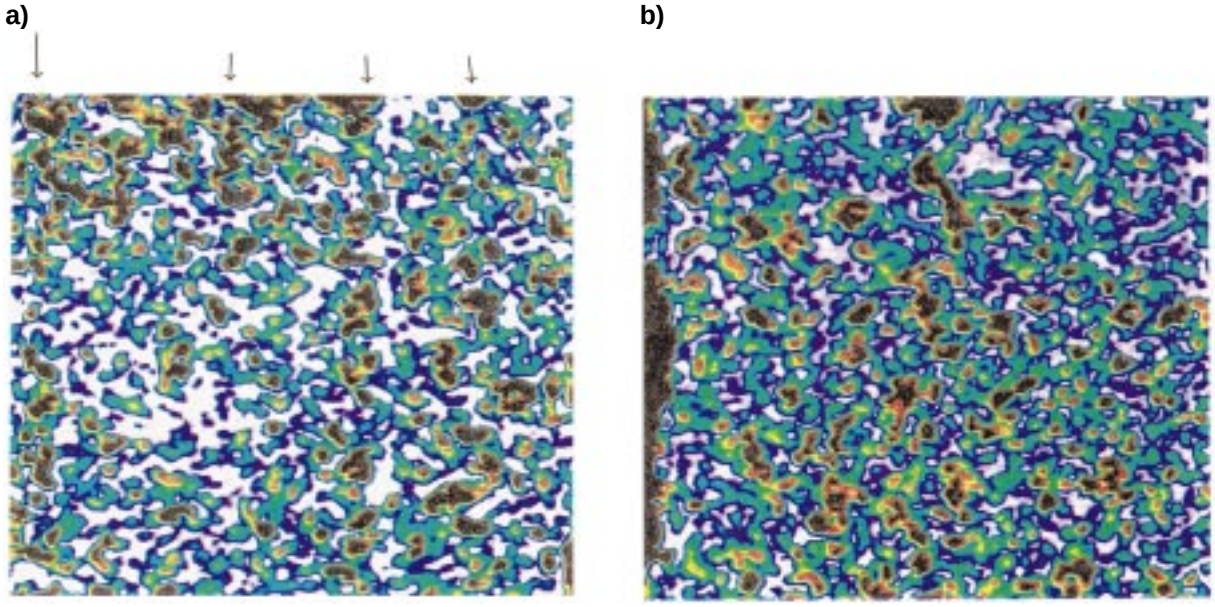

FIG. 8. Acoustic microscopy micrographs of Berea sandstone made at low frequency (25 MHz). Images of two faces are shown: (a) cut perpendicular to bedding, V_{P_h}, Q_{P_h} direction of measurement and (b) cut parallel to bedding, V_{P_v}, Q_{P_v} direction of measurement. The scanned area is 15 × 15 mm. Pore spaces are low impedance areas and are coded with darker shades and black. In (a), the arrows mark pore alignment. (b) No distinct alignment of pore spaces is observed.

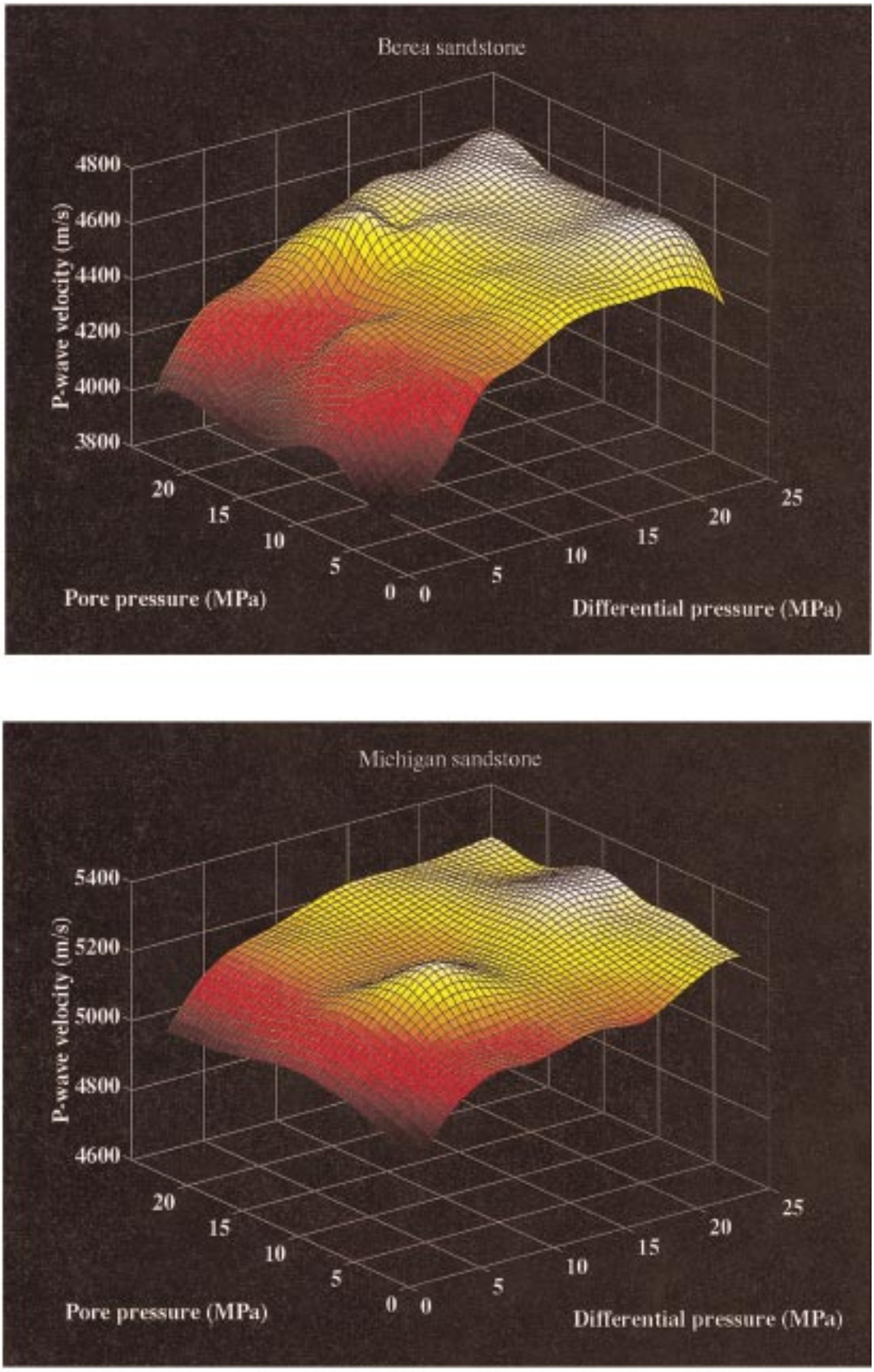

FIG. 9. Pore and differential pressure dependences of V_{P_h} in Berea and Michigan sandstones. The velocity variation is coded by a hot-color map. High velocity is marked white, low velocity is deep red.

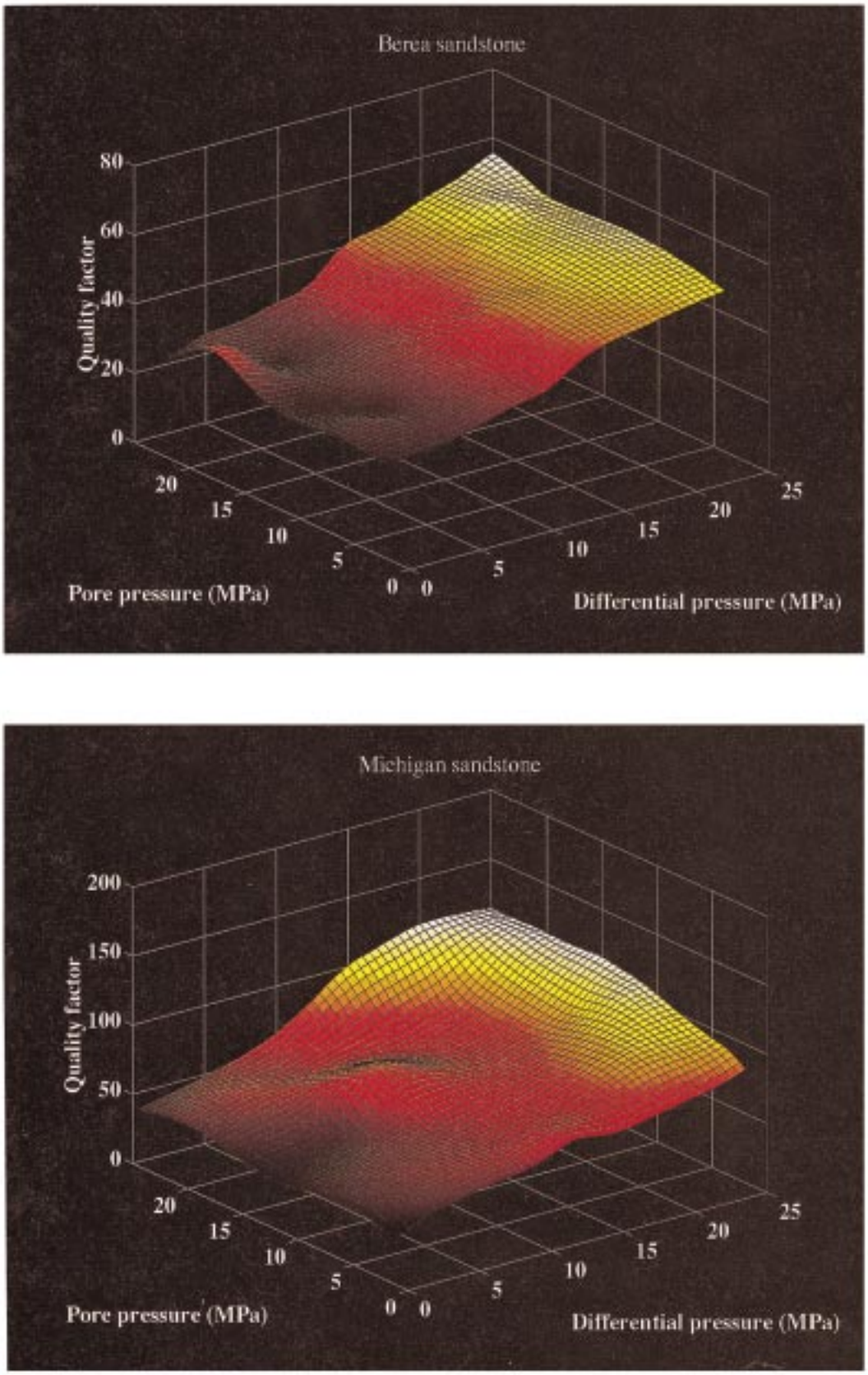

FIG. 10. Pore and differential pressure dependences of Q_{P_h} in Berea and Michigan sandstones. The quality factor variation is coded by a hot-color map. High Q_{P_h} is marked white, low Q_{P_h} is deep red.

values of n decrease with pressure for both samples (Table 3). At lower pressures (to 10 MPa), $n \approx 1$ and decreases to values of about 0.7 at 25 MPa.

In Figures 13 and 14, the separation between the P_d = constant curves becomes narrower at higher pressures. Also, the slopes of the curves increase with pressure. At low pressures (up to 10 MPa), the V_P and Q_P curves (at P_d = constant) are almost horizontal and $n \approx 1$. At higher pressures, the slopes of V_P and Q_P curves (at P_d = constant) are higher and n decreases with increasing pressure. This also follows from the observation that V_P and Q_P are dependent on both P_d and P_p. Batzle and Wang (1992) have analyzed the seismic properties of various pore fluids as a function of pressure and temperature. Their empirical analyses show an increase in brine bulk modulus and density with increasing confining pressure. Brine viscosity changes only by a few percent up to 50 MPa. The small change in V_P with P_p could be explained by a pressure dependence of the bulk modulus of brine that increases from about 2.2 GPa at 0.1 MPa to about 2.5 GPa at 50 MPa (Batzle and Wang, 1992). However, the strong dependence of Q_P on P_p shows that additional factors should be considered to explain our results. The differences in the pore pressure dependence of V_P and Q_P in two sandstones is caused by their different contact areas as observed in the acoustic microscopy micrographs.

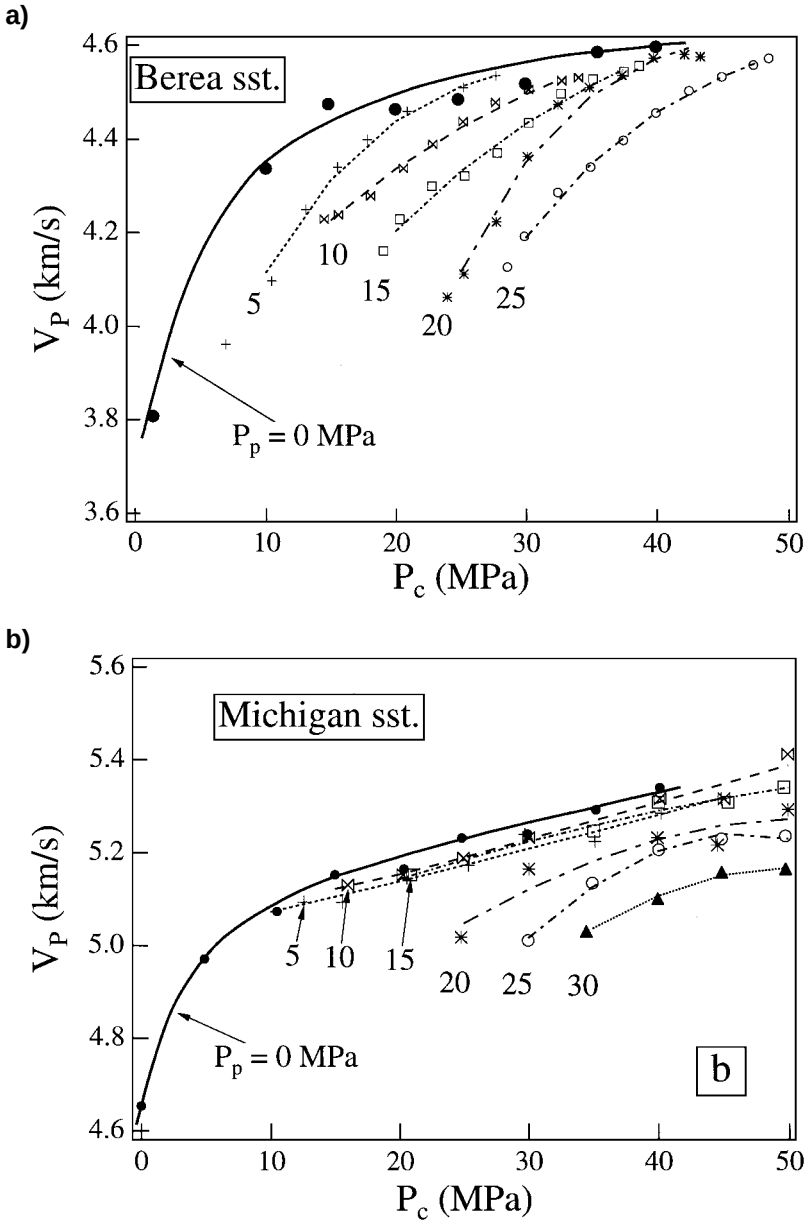

FIG. 11. V_P changes in Berea and Michigan sandstones with P_c. The data are plotted with P_p = constant. The solid and broken lines represent best fits obtained with $V^2 = A + B \cdot P_d + C \cdot e^{-P_c/D}$. P_p values for these fits are marked by numbers.

Contact areas in the Berea sandstone are wider and weaker, and appear to be somewhat interconnected (Figures 1). In Michigan sandstone, contact areas are not very wide and are not interconnected and appear as equant pores (Figure 1). This comparison between the pore spaces of the two sandstones suggests that deformation of pore space during passage of an acoustic wave is larger in Berea sandstone than in the case of Michigan sandstone.

CONCLUSIONS

The variations in V_P and Q_P as a function of confining and pore pressures for Michigan and Berea sandstones are related to differences in their microstructure. Michigan sandstone is well cemented, coarser grained, and consists of intact grains. Consequently, V_P and Q_P values are higher. Berea sandstone is fine-grained and consists of microcracks and angular grains that are poorly cemented. Thus the measured V_P and Q_P values are lower. The measured V_P and Q_P values at elevated pore pressures show that at higher pore and confining pressures, pore pressure effects do not cancel confining pressure effects. Measurements of effective stress (Christensen and Wang, 1985; Gangi, 1991; Berryman, 1992), combined with pressure-dependent properties of the pore fluid (Batzle and Wang, 1992) are needed to describe the results fully. The effective stress coefficients for both V_P and Q_P are less than 1. Compared to

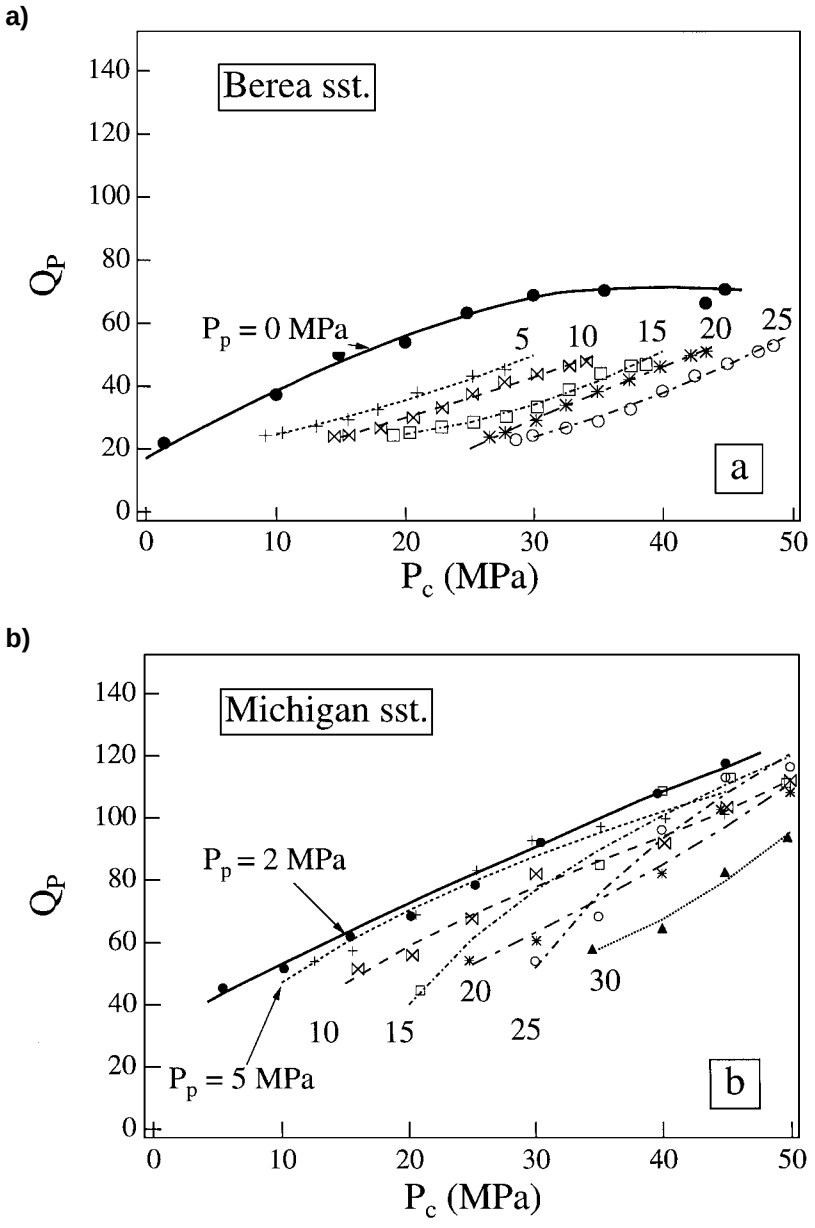

FIG. 12. Q_P changes in Berea and Michigan sandstones with P_c. The data are plotted with P_p = constant. The solid and broken lines represent best fits obtained with $Q^2 = A + B \cdot P_d + C \cdot e^{-P_c/D}$. P_p values for these fits are marked by numbers.

Table 2. Values of $[\partial V_P/\partial P_d]_{P_p}$ and n at different pressures.

	Berea sandstone				Michigan sandstone			
	$P_p = 0$		$P_p \neq 0$		$P_p = 0$		$P_p \neq 0$	
P_c (MPa)	$[\partial V_P/\partial P_d]_{P_p}$	n	$[\partial V_P/\partial P_d]_{P_p}$	n	$[\partial V_P/\partial P_d]_{P_p}$	n	$[\partial V_P/\partial P_d]_{P_p}$	n
5	4.155	0.936	4.87	0.946	3.299	0.976	3.444	0.977
10	1.809	0.985	1.96	0.986	1.413	0.932	1.334	0.928
15	0.951	0.940	1.825	0.969	0.939	0.827	1.084	0.850
20	0.628	0.747	1.121	0.858	0.815	0.836	0.789	0.831
25	0.505	0.648	0.796	0.796	0.779	0.777	0.451	0.615

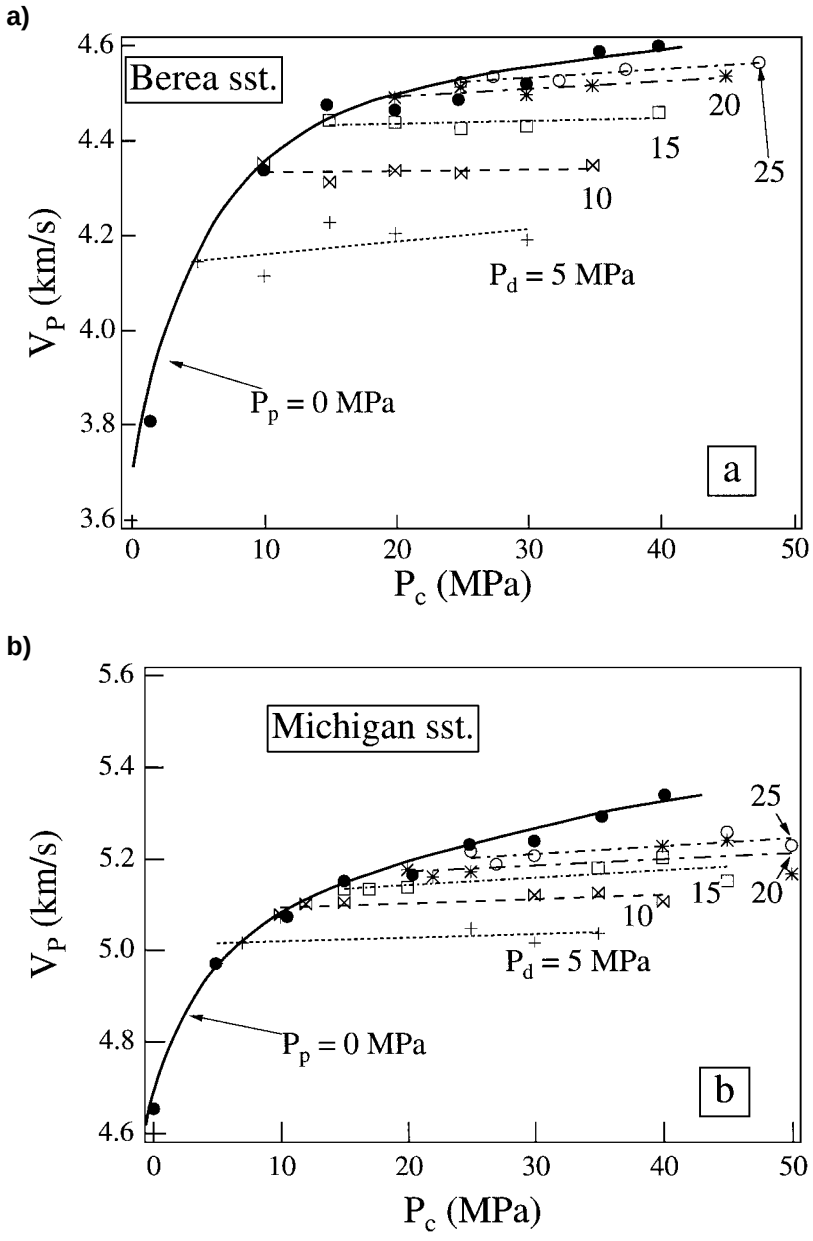

FIG. 13. V_P changes in Berea and Michigan sandstones with P_c. The data are plotted with P_d = constant. Linear fits for P_d = constant are shown by broken lines. The numbers are P_d values for each fit. The solid line represents best fit from Figure 11.

V_P, Q_P is more sensitive to variations in pore pressure and pore space deformation. The different pore pressure dependences of V_P and Q_P are explained by the type of contact areas between the grains in the two types of sandstones. Further studies of velocity and quality factor variations in other types of sandstones as a function of confining and pore pressures would also provide better understanding of the pore space deformation in such porous rocks.

Table 3. Values of *n* at different pressures.

	V_P		Q_P	
P_c	Berea	Michigan	Berea	Michigan
5	0.946	0.977	1.102	0.857
10	0.986	0.928	0.989	0.835
15	0.969	0.850	0.902	0.753
20	0.858	0.831	0.847	0.700
25	0.776	0.615	0.813	0.712

ACKNOWLEDGMENTS

John Balogh and Oliver Mathews helped in designing the experimental setup for the velocity and attenuation measurements. We thank an anonymous reviewer, Wayne Pennington, Neil Frazer, and Günter Fuchs for their valuable comments, Ingo Pecher and Günter Fuchs for developing the data acquisition program, Diane Henderson for proofreading the manuscript, and Brooks Bays for the technical drawing. This research was supported by the Petroleum Research Foundation of the American Chemical Society, grant ACS-PRF-25806-AC2, and by grants from Phillips Petroleum Company and Amoco Production Company. This is SOEST contribution no. 4118.

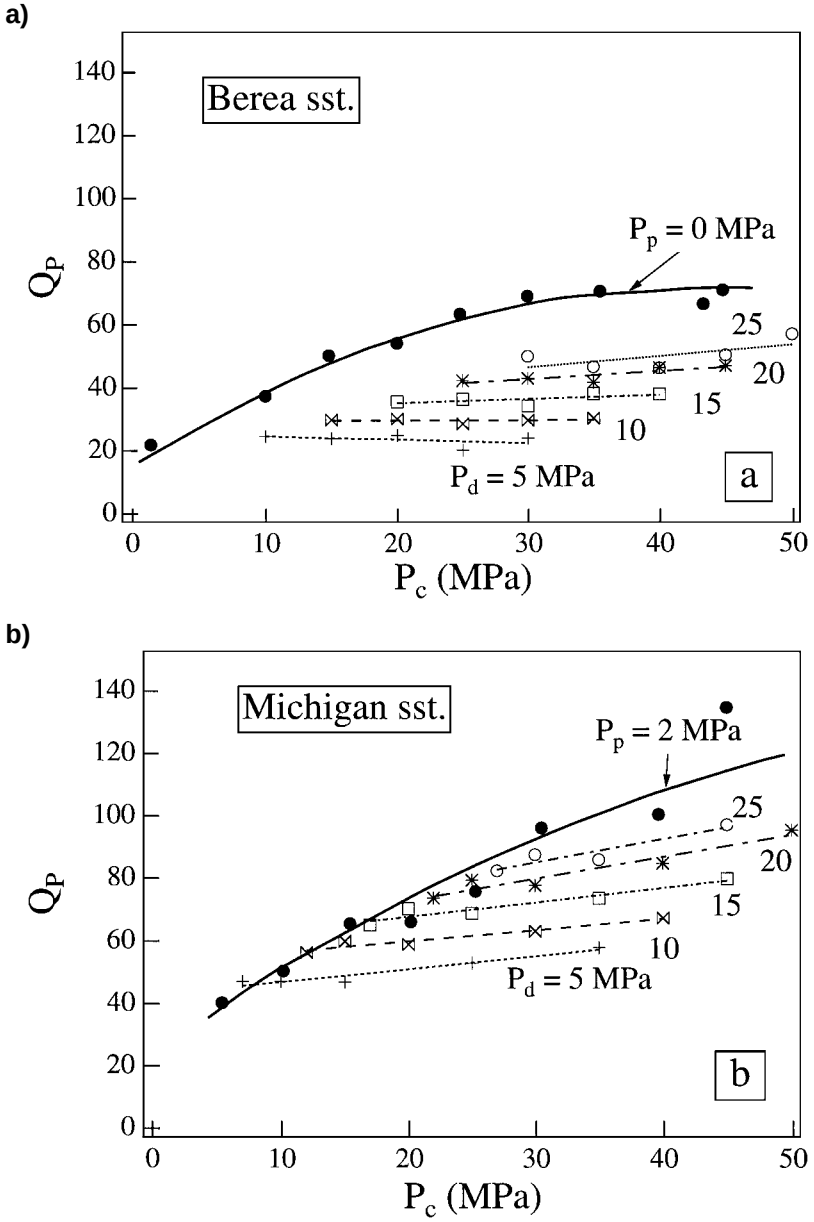

FIG. 14. Q_P changes in Berea and Michigan sandstones with P_c. The data are plotted with P_d = constant. Linear fits for P_d = constant are shown by broken lines. The numbers are P_d values for each fit. The solid line represents best fit from Figure 12.

REFERENCES

Akbar, N., Dvorkin, J., and Nur, A., 1993, Relating *P*-wave attenuation to permeability: Geophysics, **58**, 20–29.

Batzle, M., and Wang, Z., 1992, Seismic properties of pore fluids: Geophysics, **57**, 1396–1408.

Benson, G. C., and Kiyohara, O., 1974, Tabulation of some integral functions describing diffraction effects in the ultrasonic field of a circular piston source: J. Acoust. Soc. Am., **55**, 184–185.

Bernabé, Y., 1987, The effective pressure law for permeability during pore pressure and confining pressure cycling of several crystalline rocks: J. Geophys. Res., **92**, 649–657.

Berryman, J. G., 1992, Effective stress for transport properties of inhomogeneous porous rock: J. Geophys. Res., **97**, B12, 17 409–17 424.

Biot, M. A., 1956a, Theory of propagation of elastic waves in fluid saturated porous solids. I: Low frequency range: J. Acoust. Soc. Am., **28**, 168–178.

———1956b, Theory of propagation of elastic waves in fluid saturated porous solids. II: High frequency range: J. Acoust. Soc. Am., **28**, 179–191.

Birch, F., 1960, The velocity of compressional waves in rocks to 10 kilobars, Part 1: J. Geophys. Res., **65**, 1083–1102.

Brandt, H., 1955, A study of the speed of sound in porous granular media: J. Appl. Mech., Trans. Am. Soc. Mech. Eng., **22**, 479–486.

Briggs, G. A. D., 1985, An introduction to scanning acoustic microscopy: Royal Microscopical Society Handbook, **12**: Oxford University Press.

Briggs, G. A. D., 1992, Acoustic microscopy: Monographs on the physics and chemistry of materials, **47**: Oxford Science Publ.

Christensen, N. I., and Wang, H. F., 1985, The influence of pore and confining pressure on dynamic elastic properties of Berea sandstone: Geophysics, **50**, 207–213.

Coyner, K. B., and Cheng, C. H., 1985, New laboratory measurements of seismic velocities in porous rocks: Geophysics, **50**, 309.

Gangi, A. F., 1991, The effect of pore fluids and pressures on the seismic velocities in cracked and/or porous rocks: SEG Research Workshop on Lithology, Tech. Abstracts, 35–38.

Geertsma, J., 1957, The effects of fluid pressure decline on volumetric changes of porous rocks: Soc. Petr. Eng., **210**, 331–340.

Green, D. H., and Wang, H. F., 1986, Fluid pressure response to undrained compression in saturated sedimentary rock: Geophysics, **51**, 948–956.

Greenfield, R. J., and Graham, E. K., 1994, A convenient functional form, consistent with elasticity theory, for fitting velocities of rocks containing cracks: EOS, **75**, No. 16, 337.

Johnston, D. H., and Toksöz, M. N., 1980, Ultrasonic *P*- and *S*-wave attenuation in dry and saturated rocks under pressure: J. Geophys. Res., **85**, 937–942.

Jones, T., and Nur, A., 1983, Velocity and attenuation in sandstones at elevated temperatures and pressures: Geophys. Res. Lett., **10**, 140–143.

Khimunin, A. S., 1972, Numerical calculation of the diffraction corrections for the precise measurement of ultrasound absorption: Acustica, **27**, 173–181.

Lo, T.-W., Coyner, K. B., and Toksöz, M. N., 1986, Experimental determination of elastic anisotropy of Berea sandstone, Chicopee shale, and Chelmsford granite: Geophysics, **51**, 164–171.

O'Brien, D. K., Manghnani, M. H., and Tribble, J. S., 1989, Irregular trends of physical properties in homogenous clay-rich sediments of DSDP Leg 87 Hole 584, midslope terrace in the Japan trench: Marine Geology, **87**, 183–194.

Prasad, M., and Manghnani, M. H., 1996, Velocity and impedance microstructural anisotropy in reservoir rocks: 66th Ann. Internat. Mtg., Soc. Expl. Geophysicists, Expanded Abstracts, 1854–1857.

Prasad, M., Manghnani, M. H., and Siegesmund, S., 1994, Velocity and attenuation characteristics of selected KTB core samples: Scientific Drilling, **4**, 221–231.

Prasad, M., and Meissner, R., 1992, Attenuation mechanisms in sands: laboratory versus theoretical (Biot) data: Geophysics **57**, 710–719.

Rodriguez-Rey, A., Briggs, G. A. D., Field, T. A., and Montoto, M., 1990, Acoustic microscopy of rocks: J. Microsc., **160**, 21–30.

Sears, F. M., and Bonner, B. P., 1981, Ultrasonic attenuation measurement by spectral ratio utilizing signal processing techniques: IEEE Trans. on Geoscience and Remote Sensing, **GE-19**, 95–99.

Stoll, R. D., 1989, Sediment acoustics: Lecture notes in earth sciences, 26, Springer Verlag.

Todd, T., and Simmons, G., 1972, Effect of pore pressure on the velocity of compressional waves in low-porosity rocks: J. Geophys. Res., **77**, 3731–3743.

Toksöz, M. N., Johnston, D. H., and Timur, A., 1979, Attenuation of seismic waves in dry and saturated rocks, I. Laboratory measurements: Geophysics, **44**, 681–690.

Wepfer, W. W., and Christensen, N. I., 1990, Compressional-wave attenuation in oceanic basalts: J. Geophys. Res., **95**, 17 431–17 439.

Winkler, K. W., 1983, Contact stiffness in granular porous materials. Comparison between theory and experiments: Geophy. Res. Lett., **10**, 1073–1076.

———1985, Dispersion analysis of velocity and attenuation in Berea sandstone: J. Geophys. Res., **90**, 6793–6800.

———1986, Estimates of velocity dispersion between seismic and ultrasonic frequencies: Geophysics, **51**, 183-189.

Winkler, K. W., and Plona, T. J., 1982, Technique for measuring ultrasonic velocity and attenuation spectra in rocks under pressure: J. Geophys. Res., **87**, 10 776–10 780.

Zoback, M. D., and Byerlee, J. D., 1975, Permeability and effective stress: Bull. Am. Assoc. Petr. Geol., **59**, 154–158 .